
This is an electronic reprint of the original article.
This reprint may differ from the original in pagination and typographic detail.

Lastovets, Natalia; Kosonen, Risto; Mustakallio, Panu; Jokisalo, Juha; Li, Angui
Modelling of room air temperature profile with displacement ventilation

Published in:
International Journal of Ventilation

DOI:
[10.1080/14733315.2019.1579486](https://doi.org/10.1080/14733315.2019.1579486)

Published: 02/04/2020

Document Version
Peer-reviewed accepted author manuscript, also known as Final accepted manuscript or Post-print

Published under the following license:
Unspecified

Please cite the original version:
Lastovets, N., Kosonen, R., Mustakallio, P., Jokisalo, J., & Li, A. (2020). Modelling of room air temperature profile with displacement ventilation. *International Journal of Ventilation*, 19(2), 112-126.
<https://doi.org/10.1080/14733315.2019.1579486>

This material is protected by copyright and other intellectual property rights, and duplication or sale of all or part of any of the repository collections is not permitted, except that material may be duplicated by you for your research use or educational purposes in electronic or print form. You must obtain permission for any other use. Electronic or print copies may not be offered, whether for sale or otherwise to anyone who is not an authorised user.

Modelling of room air temperature profile with displacement ventilation

An accurate temperature gradient calculation is essential for displacement ventilation (DV) system design, since it directly relates to the calculation of supply air flow rate. Several simplified nodal models were developed and implemented in the various building simulation programmes to estimate the temperature stratification in rooms with displacement ventilation. However, the most commonly used models do not take into account the types and locations of the heat loads in rooms with DV. As a result, the calculated air temperature in the occupied zone can differ from the real one by 2-3 °C, which causes poor thermal comfort and inadequate sizing of the ventilation and cooling systems.

In the present study, the nodal model was proposed to provide a simplified technique to predict the vertical temperature gradient in rooms with DV. In addition, the effect of the room height and locations of the indoor heat sources were studied for the typical office environment. The measurement data were compared with the existing nodal models and the proposed nodal model in terms of predicting the occupied zone temperatures. The presented nodal model demonstrates an accurate calculation of the temperature gradient for the typical heat loads and combinations of them.

Keywords: displacement ventilation, thermal plume, mixing height, nodal model, temperature gradient

1. Introduction

In displacement ventilation (DV) systems cool air is supplied into the occupied zone of the room near the floor at low velocity and then entrained by buoyant plumes over any warm objects. As a result, a two layer room air temperature profile, stratified and mixed, is developed. Ideally, the air movements induced by thermal plumes transport heat and pollutants to the layer above the occupied zone, promoting a vertical temperature and contaminants stratification. The transition level between a mixed upper layer and stratified layer is called mixing height, which is related to the height where the inflow rate matches the airflow induced by the thermal plumes in the occupied zone. Controlling the

mixing height position is one of the most challenging tasks in DV system design, since it directly relates to the calculation of supply air flow rate.

Two different approaches were applied to control the supply airflow rate (Kosonen, Melikov, Mundt, Mustakallio, & Neilsen, 2017): a temperature based design where the design criterion is the room air temperature in the occupied zone; and an air quality based design where the design criterion is contaminant level over the occupied zone. An air quality based approach is typically used in industrial applications where the contaminant stratification is significant for DV design. In commercial buildings where the thermal comfort is the main issue, the temperature based design is the most common method. The present research focuses on commercial buildings where the temperature gradient calculation is applied to calculate an air flow rate of DV systems.

Several simplified models have been developed with nodal and zonal approach (Griffith, 2002). Zonal models solve energy balance in well-defined controlled volumes focusing on fluid balance relations. Since these models are usually applied in DV design to solve indoor air quality issues (Dokka, 2000), the present study focuses on the temperature-based models with nodal approach.

Nodal models are the analytical energy balance models with lumped parameters that treat the building room air as an idealized network of nodes connected with flow paths. They are widely applied in building design because of their simplicity, flexibility and applicability. They differ in the number of nodes, flow and heat load configuration and mixing height consideration. The models with two air nodes (Mundt, 1996; Li, Sandberg, & Fuchs, 1992; Arens, 2000) predict the linear slope between the air nodes near the floor and exhaust one. The multi-nodal models introduce the temperature profile composed by variable slopes between the nodes. These models can use precalculated air flow rates (Rees & Haves, 2001) or empirical coefficients (Mateus, & da Graça, 2015; Chen

et al., 1999) to predict the air-temperature distribution and the division of the heat loads. The above mentioned models are currently used in DV design and available in thermal energy simulation tools. The Mundt and the Mateus models are implemented in EnergyPlus, and the Mundt model is also available in IDA ICE.

The prediction of the mixing or neutral height, the level above which the temperature remains the same, is essential for all the multi-nodal models. It can be found from the plume theory (Hunt, & Van den Bremer, 2011) as a height where the air flow rate of the plume is equal to the room air flow rate. However, plume theory is valid only for the fully developed plumes. The various researches indicate that convective plumes are getting fully-developed at the height above at least three source diameters above the source itself (Menchaca-Brandan, 2012). That means that existing plume models may not be sufficient for describing buoyant plumes in low-ceiling rooms. In addition, it is important to check whether buoyancy forces are dominant in rooms with DV, since the high turbulence significantly affects the indoor air distribution (Espinosa, & Glicksman, 2017). The relation between buoyancy forces and inertia forces in ventilated rooms is described by Archimedes number (Neilsen, 2003). In the present study, the conclusions related to the applicability of plume models and the effect of Archimedes number on the temperature gradient in rooms with DV are made based on the previous studies and experimental results.

Validation and development of all those models has been based mainly on measurement with low ceiling (below 3 m). The results for low-ceiling rooms were applied in dimensionless form. However, measurements depict that modelled non-dimensional temperature profile with low ceiling height is not valid with high ceiling applications (Kosonen, 2015). Therefore, there is a need to check the effect of different ceiling height on the temperature gradient in rooms with different heights. The multi-node models are able to

provide the accurate temperature gradient prediction (Mateus, & da Graça 2015). However, for cases with high level flow elements, which are typical for commercial spaces, it was revealed that all the current models provide the incorrect results (Kosonen et al, 2015). In addition, the distribution of heat loads between the nodes still needs a deeper comprehension for better gradient prediction. Thus, there is a need to introduce a new model to calculate temperature gradient in rooms with DV.

All the current nodal models have been validated only for the simple heat load configurations and room layout. Therefore, considering the limitation of simplified models to predict temperatures in space, the model needs to be validated with temperature measurements in different part of the room with DV. The nodal model proposed in the present study is developed and validated with the measurement results for office layouts with different arrangement and sources of heat loads.

2. Methods

This section describes the mixing height calculation methods for different heat sources and compares the chosen nodal models with the presented one in terms of their structure and performance. Then the validation of all the models with experimental results of the two measurement setups is provided.

2.1 Methods to calculate the mixing height

Since fluid flow in displacement ventilation is driven by convective flows from the heat sources, plume theory is widely applied in the temperature gradient calculation. The sources of indoor heat loads normally differ in geometrical shape, heat loss and location. Plumes in rooms most commonly have a circular cross-section, since heat sources are three-dimensional. Fully-developed round buoyant plumes in a uniform environment has a closed analytical solution for volumetric flowrate, momentum and buoyancy flux

(Hunt, & Van den Bremer, 2011). In addition, the experiments indicate that the volumetric flowrates from plume sources of different geometrical forms are very similar (Zukowska, Melikov, & Popiolek, 2007; Menchaca-Brandan, 2012). Therefore, the point source method can be applied to the heat sources close to cylindrical and rectangular shape (Fontaine, Devienne, & Rose, 2006). The mixing height of convection plumes is obtained from the equality of room air flow and total air flow across a horizontal cross-section of a plume. In the case of multiple plumes from vertical heat sources the mixing height is determined from the following equation:

$$h_{\text{mx}}^{\text{ver}} = (k_q^{\text{p}})^{-\frac{3}{5}} \cdot \left(\frac{q_v}{n}\right)^{\frac{3}{5}} \cdot \Phi_c^{\frac{1}{5}} + h_0^{\text{ver}} \quad (1)$$

where: q_v is a volume flux (m^3/s), Φ_c is a convective heat (W), n is an amount of plumes, h_0^{ver} is a virtual origin height (m), k_q^{p} is an entrainment coefficient for a point source plume.

The entrainment coefficient depends on profile assumptions in integral plume models and air properties. However, both theoretical (Davidson, 1986) and experimental studies (Blaise, 2008) indicate that the entrainment coefficient k_q^{p} has a main value 0.005 with an error in the fourth digit after the decimal point.

Location of virtual origin is defined as the distance of a point source from the surface of a real source, so that the point source generates the same velocity and temperature profiles as the real source. The location of the virtual point is usually dependent on the geometrical parameters of the heat source and the selected parameters of virtual origin setting (Hunt, & Kaye, 2001). The different techniques to calculate the location of virtual origin for vertical sources are shown in Table 1:

Table 1. Virtual origin calculation for vertical plume sources.

Method		Simplified formula
Conical correlation	Morton (Morton,1959)	2,28D
	Skistad maximum (Skistad,1994)	2.26D
	Skistad minimum (Skistad,1994)	1.47D
Source correlation (Mundt,1996)		2.09D+ 0.2(Hs/ΔT)0.25
Experimental and numerical studies (Menchaca-Brandan,2012)		1.48D

H_s and D are correspondently the height and the diameter of the source (m). ΔT is a temperature difference between the source and the ambient air (K).

Among the above mentioned methods, the present study applies the conical correlation with “minimum” approach (Skistad, 1994) to calculate the virtual origin height above the vertical heat source:

$$h_0^{ver} = H_s - 1.47 \cdot D \quad (2)$$

To calculate the thermal plume from the rectangular source, the diameter is replaced by hydraulic diameter of the top of the source.

The buoyancy plume parameters from horizontal heated surfaces are less studied and still required more research (Chaengbamrung, 2005). The plume height in this case is dependent on the geometry of this source. The point source formula for the mixing height works with round shape sources or the rectangular ones with the aspect ratio (length/width) less than 2. In the case when the aspect ratio is greater than 2, the formulae corresponding to a linear source must be considered (Devienne, & Fontaine, 2012).

The virtual origin setting for the horizontal area source could be calculated with the correlation for area source plume with “neck” (Kaye & Hunt, 2009) that also fits the experimental studies (Bouzinaoui, Devienne, & Fontaine, 2007). However, the previous studies revealed that these models are only applicable to the relatively small horizontal heat sources. The transition from displacement to mixing ventilation occurs when the area of the source exceeds 15% of the floor area or even significantly less (Kaye, & Hunt, 2010).

The mixing height from the convection vertical surface usually occurs in a high zone of a room. However, first temperature near the heated vertical surface happens due to the flow transition from laminar to turbulent regime (Cooper, Hunt, & Linden, 2001). The transition level can be estimated considering the condition for changing the flow regime from laminar to turbulent: $Gr \cdot Pr = 7 \cdot 10^8$:

$$h_{tr}^{v,surf} = \left(\frac{7 \cdot 10^8 \cdot \nu \cdot k}{g \cdot \beta \cdot (\theta_w - \theta_{sur}) \cdot c_p \cdot \rho} \right)^{1/3} + H_w \quad (3)$$

where: ν is a kinematic viscosity (m^2/s); k is a thermal conductivity ($W/(m \cdot K)$); g is a gravity acceleration (m/s^2); θ_w is a temperature of the window surface ($^{\circ}C$); θ_{sur} is a surrounding temperature ($^{\circ}C$); c_p is a heat capacity ($W/(m^2 \cdot ^{\circ}C)$); H_w is a height of the bottom of the window (m); ρ is a density (kg/m^3); β is a thermal expansion coefficient ($1/K$).

In order to count the strengths of different heat sources located in the room with DV, the weight factors of the corresponding heat loads is proposed in this study:

$$h_{mx} = h_{mx}^{ver} \cdot \frac{\Phi_c^{ver}}{\Phi_c} + h_{tr}^{v,surf} \cdot \frac{\Phi_c^{v,surf}}{\Phi_c} \quad (4)$$

where Φ_c is the total convective heat load (W).

2.2 Nodal models to predict the temperature gradient

Four nodal models with different approaches were chosen to be analysed and compared with the proposed one: the Mundt, the Nielsen, the Rees & Haves and the Mateus 3-nodal model. Mundt (Mundt, 1996) proposed the 2-nodal model where temperature gradient is calculated to be linear over the room height. In this model the radiative energy flux from the floor is balanced by convective heat transfer from the floor surface to the air. In the Nielsen model (Nielsen 2003) the linear vertical temperature gradient between floor and the height of mixing layer is predicted with Archimedes number and the type

of heat load. The mixing height is calculated for a point source in stratified environment. A simplified three-nodal model was proposed by Mateus and da Graça (Mateus, & da Graça, 2015) with the use of load separation and low zone mixing factor. In addition, this model calculates the temperatures of wall surfaces: floor, ceiling, high and low levels of the walls. The alternative approach to consider the flow patterns between nodes was developed by Rees and Haves (Rees & Haves, 2001). The model includes 11 interrelated nodes: 4 room air nodes out of the thermal plume, 4 nodes of the air flow within the plume and 3 surface nodes representing floor, ceiling and wall temperatures. In addition, this model uses 14 flow paths between the nodes with flow rate parameters that are pre-determined by experimental and numerical studies.

The nodal model (Figure 1) predicts room air temperature at three heights: at the height of 0.1 m, at the height of the mixed layer (h_{mx}) and the height of the exhaust air temperature that is equal to the room height. Heat load distribution determines the convection heat transfer connection between the wall and air nodes. Low heat loads are considered to be the ones that occur in the occupied zone of the room, whereas high heat loads are located near the ceiling. The examples of low heat loads are the ones from people and office equipment. The high heat loads in practice could be from lighting units, heated ceiling or solar gains through high-located windows. When heat load occurs in the middle of the room, it depends on the mixing height whether consider them high or low heat loads. If the mixing height is located within the occupied zone, it refers to low heat loads, and vice versa.

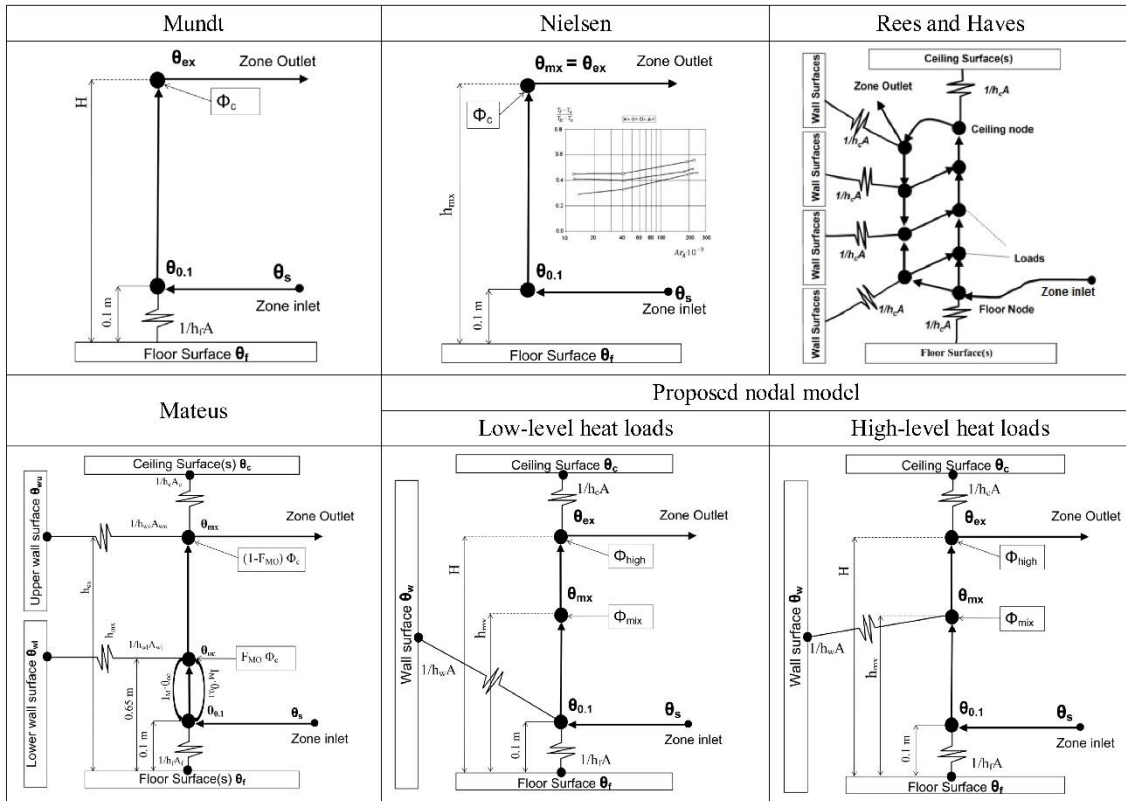


Figure 1. Simplified nodal models to calculate a temperature gradient in rooms with DV. The model consists of the set of 3 convection and 3 radiation heat balance equations assuming 50% split between the convective and radiative heat loads. The airflow pattern is predefined in the model, so that the air-distribution in the room is displacement. However, dominated high-level heat loads and long-wave radiation heating up the room surfaces in the occupied zone affect the airflow patterns and temperature gradient. The proposed model allows calculating the case when high-heat loads are presented, but not dominated in the indoor heat balance. The cases when dominated high-located heat loads that not covered by the simplified nodal model are described as the limitations of the model in Discussion section.

The convective heat balance in three nodes includes the following equations (Eq.5-7) for the case, when the most heat loads are located in the lower zone of the room:

Near the floor level:

$$\rho \cdot c_p \cdot q_v \cdot (\theta_{0.1} - \theta_s) = \alpha_{cf} \cdot A_f (\theta_f - \theta_{0.1}) + \alpha_w \cdot A_w \cdot (\theta_w - \theta_{oc}) \quad (5)$$

Mixing level:

$$\rho \cdot c_p \cdot q_v \cdot (\theta_{mx} - \theta_{0.1}) - \rho \cdot c_p \cdot q_v \cdot (\theta_e - \theta_{mx}) = \Phi_{mx} \quad (6)$$

Wall surface:

$$\alpha_{c,w} \cdot (\theta_w - \theta_{0.1}) + \alpha_{r,w} \cdot (\theta_w - (\theta_c A_c + \theta_f A_f) / (A_t - A_w)) = \Phi_r / A_t \quad (7)$$

In the case, when the most heat loads are located in the upper zone of the room, the equations of 8-10 should be used:

$$\rho \cdot c_p \cdot q_v \cdot (\theta_{0.1} - \theta_s) = \alpha_{cf} \cdot A_f (\theta_f - \theta_{0.1}) \quad (8)$$

$$\rho \cdot c_p \cdot q_v \cdot (\theta_{mx} - \theta_{0.1}) = \Phi_{mx} + \alpha_w \cdot A_w \cdot (\theta_w - \theta_{mx}) \quad (9)$$

$$\alpha_{c,w} \cdot (\theta_w - \theta_{0.1}) + \alpha_{r,w} \cdot (\theta_w - (\theta_c A_c + \theta_f A_f) / (A_t - A_w)) = \Phi_r / A_t \quad (10)$$

The exhaust, floor and ceiling surface nodes of the model remain the same for the both cases:

$$\rho \cdot c_p \cdot q_v \cdot (\theta_e - \theta_s) = \Phi_{tot} \quad (11)$$

Floor surface:

$$\alpha_{c,f} \cdot (\theta_f - \theta_{0.1}) + \alpha_{r,f} \cdot (\theta_f - (\theta_c A_c + \theta_w A_w) / (A_t - A_f)) = \Phi_r / A_t \quad (12)$$

Ceiling surface:

$$\alpha_{c,c} \cdot (\theta_c - \theta_e) + \alpha_{r,c} \cdot (\theta_c - (\theta_f A_f + \theta_w A_w) / (A_t - A_c)) = \Phi_r / A_t \quad (13)$$

where: q_v is the air flow rate (m^3/s), θ_e is the exhaust air temperature ($^{\circ}C$), θ_f is the average temperature of the floor ($^{\circ}C$), θ_w is the average temperature of the wall ($^{\circ}C$), θ_c is the

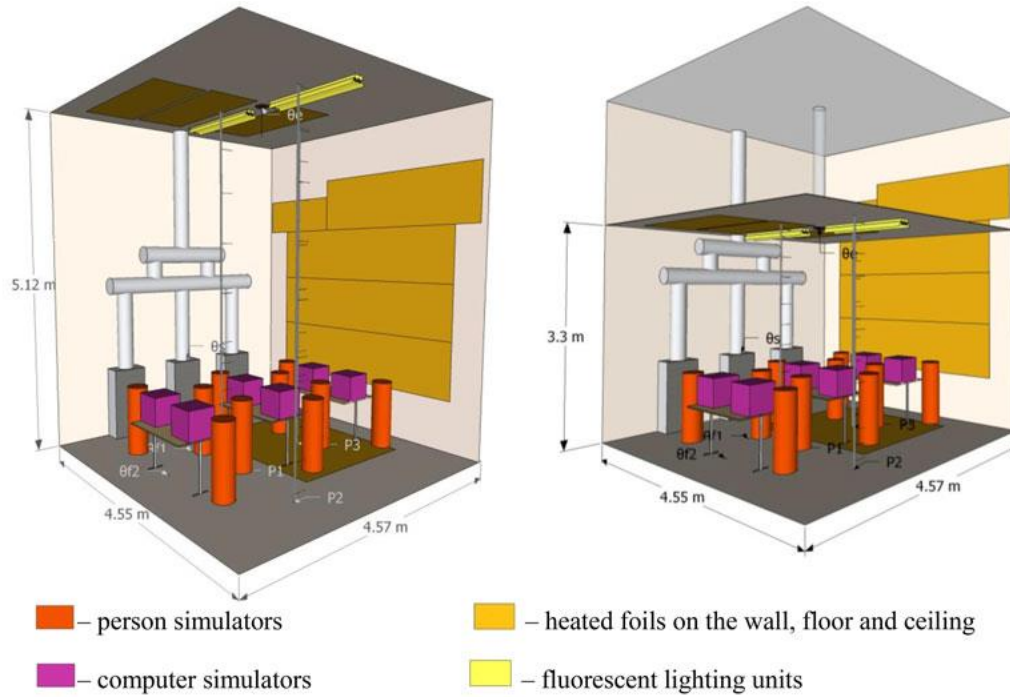
average temperature of the ceiling ($^{\circ}\text{C}$), Φ_{mx} are the convective heat loads under the mixed layer (W), Φ_{high} are the convective heat load over the mixed layer (W), $\alpha_{c,c}$, $\alpha_{c,f}$ and $\alpha_{c,w}$ ($\text{W}/(\text{m}^2\cdot^{\circ}\text{C})$) are the convective heat transfer coefficients of the room surfaces: ceiling, floor and wall surfaces.

The proposed equations are linear if the heat transfer coefficients are constant. In a case when correlations for convective heat transfer coefficients are applied (Novoselac A, Burley BJ, & Srebric J., 2006), the equations are getting non-linear and required iteration methods to solve it.

2.3 Validation of the nodal models

Two test setups are applied to validate the chosen currently used nodal model and the presented one. The first one is focused on the analysis of different heat sources, air flow rates and room heights on the temperature gradient with DV. The second one performed in different office layouts includes 10 measuring points that allows studying the uniformity of vertical temperature gradient throughout the room.

The test setup to check the model calculation in rooms with different flow elements consists of displacement diffusers with perforated front face and ceiling exhaust in insulated with 100 mm polystyrene room with 20.8 m^2 floor area and room height of 5.12 m. The internal heat loads (Table 1) consist of heated cylinders representing persons, heated cube-shaped boxes representing computers, heated foils in one wall and ceiling representing solar load on window at different levels and fluorescent lighting units (Figure 2). The computer simulators are made of non-painted galvanized steel. Personal simulators are made of galvanized steel and painted grey.



Measurement points: P1, P2, P3 – room air temperatures; θ_{f1} , θ_{f2} – floor surface temperatures; θ_s – supply air temperature; θ_e – exhaust air temperature

Figure 2. Measurement setup to study the effect of different room heights and heat loads

The Archimedes number is calculated for every case (Table 2, 3) to analyse the influence of the relation between buoyancy and inertia forces to the vertical temperature gradient:

$$Ar = \frac{\beta g H \Delta T_0}{\left(\frac{q_0}{A}\right)^2} \quad (14)$$

where: β is the thermal expansion coefficient (1/K), g is the acceleration of gravity (m/s^2), H is the room height (m), ΔT_0 is the difference between the exhaust and supply air temperatures (K), q_0 is the airflow rate to the room (m^3/s), A is the floor area of the room (m^2).

The temperature profiles are measured from four locations (P1-P4 in Fig.2) at ten heights with calibrated PT100 sensors (accuracy ± 0.2 °C). Surface temperatures were measured with Testo 830-TI-infrared thermometer (accuracy ± 0.1 °C). Supply and exhaust air flows were measured with air flow rate measurement device MSD 100, that was

calibrated with an orifice plate to reach the accuracy $\pm 3\%$. Airflow measurement of MSD device is based on differential pressure created by measurement probe pipes. The airflow rate $0.05 \text{ m}^3/\text{s}$ was measured with Halton MSD 100 and MSD 200 and the airflow rate $0.15 \text{ m}^3/\text{s}$ was measured with MSD 200. The devices were located in ductwork on top of measurement room.

Table 2. Measured buoyant flow elements and heat load combinations.

Case	Heat loads, W							Supply temperature, room height 5.12/3.3 m °C	Supply air flow rate m^3/s	Air $\times 10^3$
	Heated Cylinders	Heated Boxes	Foils on the wall	Foils on the floor	Foils on the ceiling	Lighting units	Total heat loads W			
Single loads										
a 6 people	450	-	-	-	-	-	450	20.6	0.05	116
b 6 computers	-	720	-	-	-	-	720	21.2	0.05	198
g 3 computers	-	360	-	-	-	-	360	19.4	0.15	5
	-	360	-	-	-	-	360	19.9	0.05	99
h Ceiling heat loads	-	-	-	-	466	-	466	19.5	0.15	19
	20.1	-	-	-	466	-	466	21.1	0.05	139
i Window heat loads*	-	0.05	79	-	-	-	520	20.5	0.05	96
	18.9	117	-	-	-	-	520	20.7	0.05	14
Window heat loads**	-	-	520	-	-	-	520	18.9	0.15	7
j Window heat loads*	-	-	520	-	-	-	520	19.1	0.15	8
Window heat loads**	19.8	3	-	-	-	-	520	18.1	0.1	57
Combinations of heat loads										
c 6 people, 6 computers	450	720	-	-	-	-	1170	18.1	0.1	83
d 10 people, window*** and floor heat loads	750	-	520	466	-	-	1736	16.3	0.1	83
e 10 people, window*** and heat loads, lighting	750	-	520	-	-	235	1505	16.6	0.1	72
f 10 people, ceiling heat loads	750	-	-	-	466	-	1216	16.6	0.1	69
k 10 people, lighting	750	-	-	-	-	232	982	17.2	0.1	48
l 10 people, ceiling heat loads, lighting	750	17.7	11	-	-	-	1448	16.7	0.1	72
m 10 people, window*** and floor heat loads, lighting	750	17.7	40	260	-	-	1762	15.9	0.1	85
n 10 people, window*** and floor heat loads, lighting	750	18.1	520	260	51	-	1762	17.2	0.18	15
	750	-	520	260	-	-	1762	18.2	0.18	9

*Window height $h_w=1.8 \text{ m}$ at initial level of 0.8 m over the floor.

**Window height $h_w=3.6 \text{ m}$ at initial level of 0.8 m over the floor.

***Window height $h_w=3.6 \text{ m}$ when $H=5.1 \text{ m}$, $h_w=1.8 \text{ m}$ when $H=3.3 \text{ m}$.

In addition, the model was validated with the experimental results published by Arens (Arens, 2000) for open-plan and cubicle-style office arrangements (Table 3). The test room layout is shown in the Figure 3.

Table 3. Measured buoyant flow elements and heat load combinations.

Case	Heat loads, W			Total heat loads W	Aver sup temper
	Heated rectangular-shaped boxes	Heated square-shaped boxes	Lighting units		
Open-plane office, Cubicle-style office 4 people, 4 computers, lighting units	360	300	732	1392	15

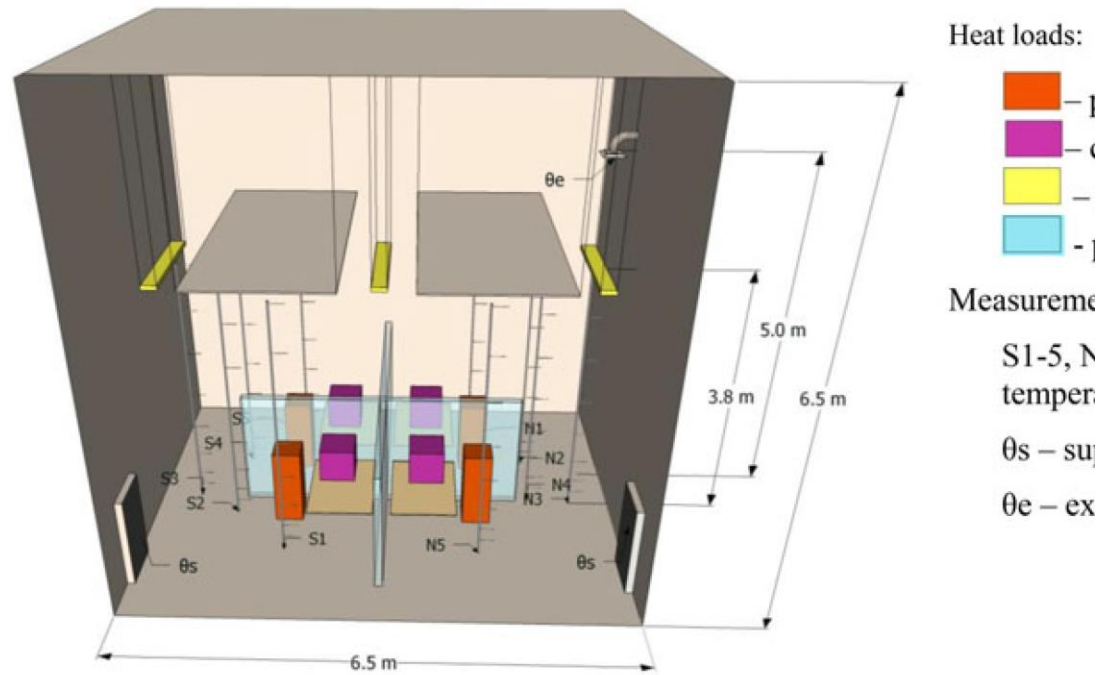


Figure 3. Measurement setup to study the effect of different room heights and heat loads.

The supply air is delivered from two opposing air distributors, whereas the exhaust grille is located overhead to the right at height of 5 m. The internal heat loads were modelled by person and computer simulators (heated boxes) and 3 rows of lighting units. The room height is 6.5 m, whereas the fluorescent lighting fixtures were located 3.8 m above

the floor. Air temperature measurements were conducted with 0.6 mm diameter copper-constantan thermocouples with a ± 0.2 °C accuracy at each of the ten positions indicated during each test.

The supply air is delivered from two opposing air distributors, whereas the exhaust grille is located overhead to the right at height of 5 m. The internal heat loads were modelled by rectangular person and computer simulators and 3 rows of lighting units. The room height is 6.5 m, whereas the fluorescent lighting fixtures were located 3.8 m above the floor. Air temperature measurements were conducted with 0.6 mm diameter copper-constantan thermocouples with a ± 0.2 °C accuracy at each of the ten positions indicated during each test.

Thus, the validation of the model was conducted for rooms with different layout and typical heat loads in commercial building.

3. Results

The measured data of the temperature gradient for the typical indoor heat loads (Table 2,3) were compared with the calculation results of the selected simplified nodal models: the Mundt, the Nielsen, the Mateus, the Rees & Haves and the presented nodal model. The air properties are taken for standard conditions: $\rho = 1.2$ kg/m³, $c_p = 1005$ J/(kg·°C). The heat transfer coefficients in the Mateus and the presented nodal model are calculated using Novoselac correlation (Novoselac et al., 2006), whereas in the Mundt and Rees & Haves model the values recommended by the authors of these models are applied. The capacity rates in the Rees & Haves model calculation are taken as recommended by the authors (Rees & Haves, 2001). In the Nielsen model the case with computer, desk lamp and manikin is taken as a reference.

In the presented nodal model the low heat loads Φ_{mx} are from people, floor. The computers are located in the low zone of the room. The transition level of the window heat

loads is up to 2 m high, thus they were also calculated as low heat loads. The high heat loads are from the ceiling and lighting.

The results of the corresponding measurements and calculations are presented at the Figure 4 – 6. In all the figures of the temperature gradients the dimensionless temperature κ is an abscissa axis and the room height H is an axis of ordinates.

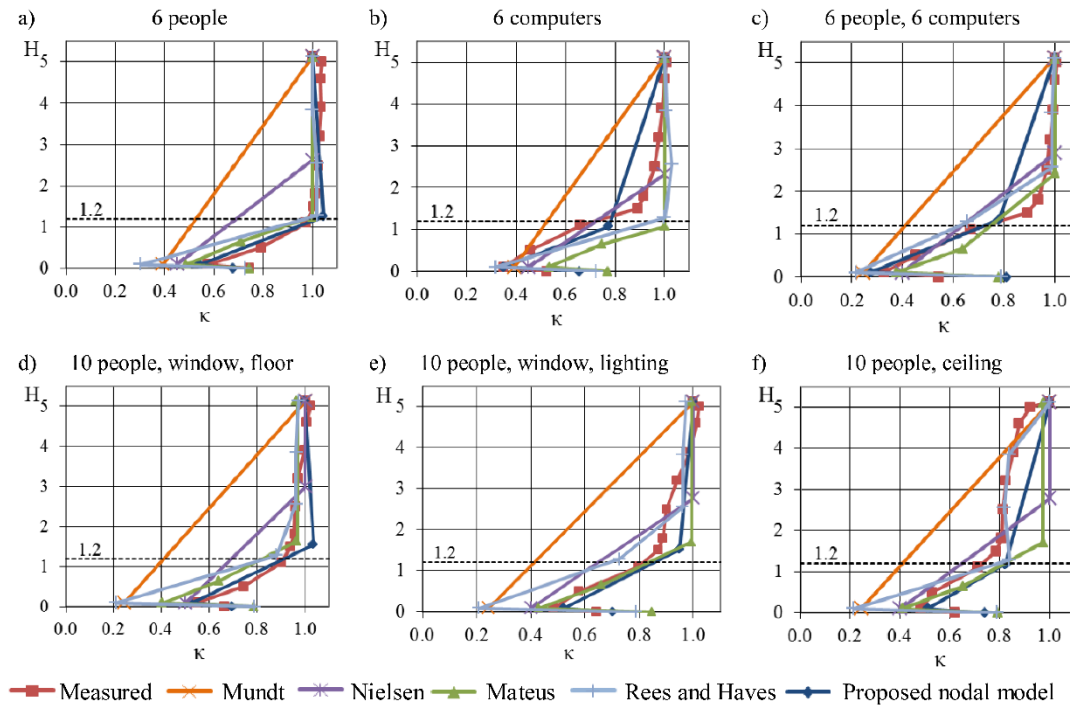


Figure 4. Comparison of the different nodal models with the measurement data.

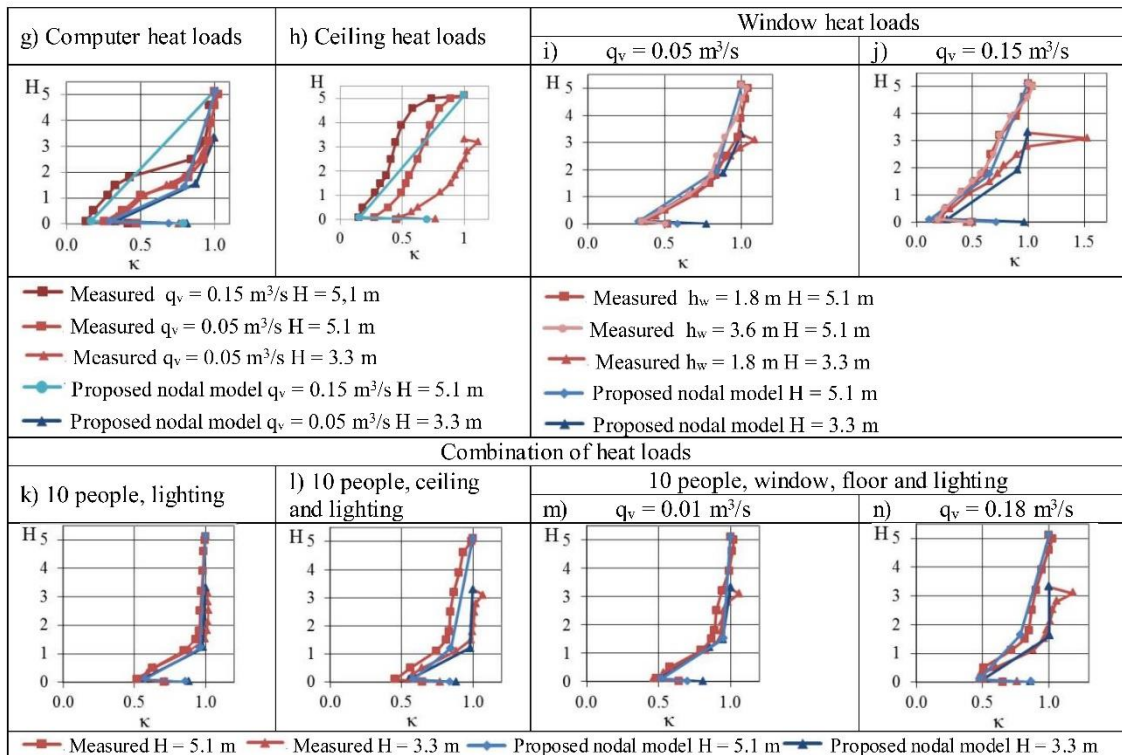


Figure 5. Measured and modelled temperature gradients for the rooms with different heights, heat loads and airflow rates (h_w is the window height, q_v is the airflow rate).

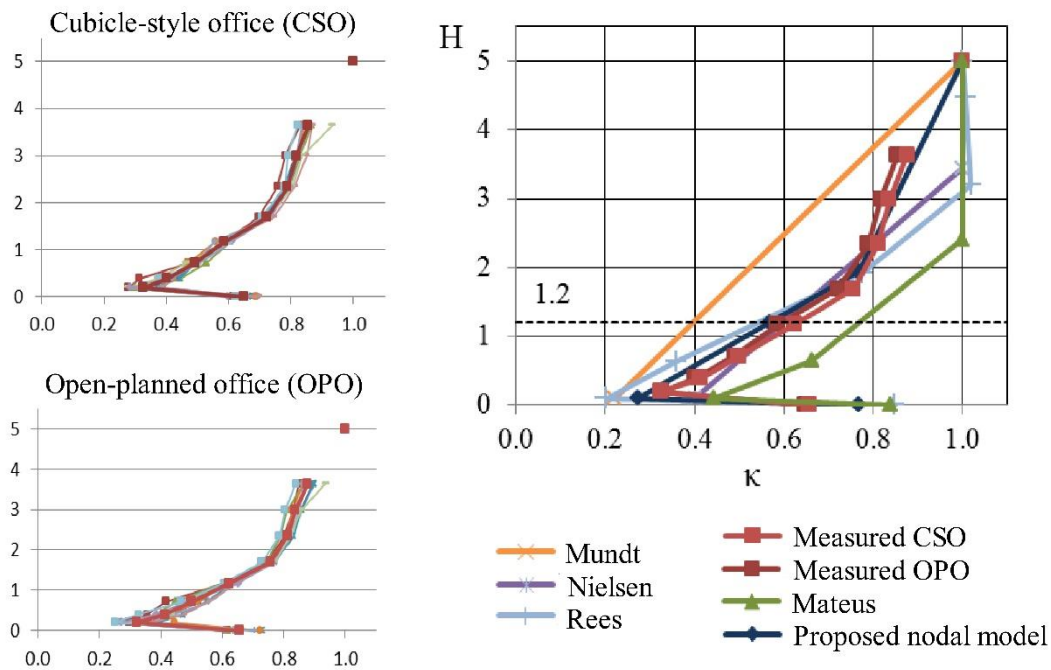


Figure 6. Measured and modelled temperature gradients in open-planned office (OPO) and cubicle style office (CSO).

3.1 Accuracy of the models

To assess the accuracy of the models the following average error indicators is used: Average norm of the error:

$$\text{Avg. Dif.} = \frac{\sum_{i=1}^n (|\text{Sim}_i - \text{Meas}_i|)}{n} \quad (15)$$

Average bias:

$$\text{Avg. Dif.} = \frac{\sum_{i=1}^n (\text{Sim}_i - \text{Meas}_i)}{n} \quad (16)$$

Average error:

$$\text{Avg. Error} = \frac{100\%}{n} \cdot \sum_{i=1}^n \left| \frac{\text{Sim}_i - \text{Meas}_i}{\text{Sim}_i} \right| \quad (17)$$

where:

Sim_i is a simulation result, °C;

Meas_i is a measurement result; °C;

n is a number of experiments.

The validation of the selected DV models was conducted based on the simulation and measurement results in three important temperatures at the heights of 0.1, 1.1 and 1.8 m. The average results of the all measured cases are presented in Table 4.

Table 4. Error indicators of the validated models.

Model	Node	Avg dif (°C)	Avg bias (°C)	Avg error (%)
Mundt	$\theta_{0.1}$	2.2	-2.2	10%
	$\theta_{1.2}$	3.4	-3.4	14%
	$\theta_{1.8}$	3.1	-3.1	12%
Nielsen	$\theta_{0.1}$	0.5	-0.3	2%
	$\theta_{1.2}$	1.4	-1.4	6%
	$\theta_{1.8}$	1.2	-1.1	4%
Mateus	$\theta_{0.1}$	0.9	-0.7	4%
	$\theta_{1.2}$	1.0	0.2	4%
	$\theta_{1.8}$	0.7	0.5	3%
Rees and haves	$\theta_{0.1}$	2.5	-2.5	11%
	$\theta_{1.2}$	1.4	1.4	6%
	$\theta_{1.8}$	0.5	0.2	2%
Proposed nodal model	$\theta_{0.1}$	0.3	0.0	1%
	$\theta_{1.2}$	0.4	0.1	2%
	$\theta_{1.8}$	0.3	0.2	1%

The two-nodal Mundt model is not able to calculate the temperature gradient for all the cases. The occupied zone temperature at the height 1.2 m calculated by the Mundt model was roughly 3°C lower than the measured one. Even though, the range of the experimental values in the Nielsen model is limited, it is able to predict the temperature near the floor; however it overestimates the mixing height level. The negative values of average bias (Table 4) indicate that Mundt and Nielsen models underestimate the air temperatures at all the levels of occupied zone of the room.

The Mateus and the presented nodal models demonstrate similar temperature gradient prediction in the cases with low level heat loads. However, unlike the cases with high level heat gains, such as heated ceiling, high window and computers, the Mateus model accurately calculates the temperature gradient in the occupied zone of the room, since it does not assume the gradient upper the mixing height. The Rees & Haves model also works well in the cases with low heat loads (Figure 4 a, d), and in some cases (Figure 4, f) the model demonstrates the ability to follow the curve of the gradient. However, the recommended (Rees & Haves, 2001) air capacities do not suit in all the combinations of internal heat loads. Thus, it requires precalculation of air capacities in every complicated case. The proposed nodal model demonstrates the average difference between the estimated and measured values 0.4 °C at the height 1.2 m.

In the cases with low level heat sources the major part of the gradient exists in the occupied zone regardless of the room height. The influence of the room height on the vertical temperature gradient is essential in the cases with high-level heat loads, when the temperature tends to stratify over the mixing level (Figure 5 1). However, for the cases with only vertical heated surfaces, air-flow rate is more influential on the temperature

gradient in the rooms with different heights (Fig.5 i, j). The height of the distributed window heat source can be neglected, since the influence of heat gain is more essential for the temperature gradient in the transition level.

The relation between buoyancy dominated to momentum dominated flows significantly affect the temperature gradient in low-ceiling rooms with high-level heat loads. The analysis of the experimental results indicate the growing influence of inflow jets when the Archimedes number is lower than roughly $10 \cdot 10^3$. In low-ceiling rooms (Fig. 5 m, n), when the impact of inflow jet is getting higher, the temperature tends to stratify over the mixing height. It practically means that in the case of high heat loads, low ceiling and/or dominated inertia forces ($Ar < 10 \cdot 10^3$) the high heat loads are getting to the mixing lever. The temperature gradient of the computer and ceiling heat loads also differ significantly depending on the airflow rates (Figure 5 g, h). Thus, in the cases of single heat loads relatively higher than floor level and dominated momentum forces the proposed model in 2 nodal mode can be still applied to predict the low-zone temperatures.

An arrangement of office layout has some effect of the thermal stratification in rooms with DV. Despite the fact that the vertical temperature gradients tend to be similar throughout the room, the office furniture that prevents even air distribution increases unevenness of temperature stratification in low zone of the room (Figure 6).

4. Discussion

Usually measurements for validation the models are conducted in low-ceiling rooms with limited heat loads sources; usually they are person and computer simulators. At the same time, in real application of displacement ventilation the heat loads are more diverse. The presented measured data cover typical heat loads from different amount of people, computers, lighting units, heated surfaces and different combinations of them. The second measurement setup allows investigating the influence of typical furniture obstacles on the

temperature gradient in different places of the room. In addition, the study of displacement ventilation in rooms with different heights shows different temperature gradient performance .

Despite the common approximation of linear temperature gradient in rooms with DV, the various measurements reveal the opposite. The results represent typical temperature stratification in rooms with displacement ventilation, when the main gradient occurs in the low zone. Thus, the models that do not count the level of stratification are not able to accurately calculate the temperature gradient. According to the measurements, two-nodal models can only predict the gradient in the case with vertical heated surfaces. The proposed model improve the temperature gradient calculation in room with DV by accounting the influence of different typical internal heat loads.

Despite their simplicity and applicability, nodal models are not universal in predicting the temperature gradient, since they are not able to count all the variety of factors affecting the indoor airflows. When internal heat gains split into several highly asymmetric plumes, it may generate a stratification profile with several mixing heights. The simplified nodal model does not cover this complicated indoor temperature distribution. The model is also inapplicable when internal heat gains are predominately radiative or located out of the occupied zone. In that case, long-wave radiation heats up the room surfaces in the occupied zone affecting the airflow patterns and temperature gradient and creating a close to linear temperature gradient without recognisable mixing height.

Thus, in the case of complicated unconventional heat load sources, uneven distribution of heat and momentum fluxes, CFD methods are more applicable.

In addition, since the model is steady-state, it is not able to count the effect of dynamic loads and thermal mass on the temperature gradient. However, in real-time building op-

eration conditions variation of heat loads and thermal mass effect have a significant influence on the temperature gradient. It could result in inadequate system operation and design. Therefore, the proposed model should be validated in the dynamic mode.

Due to the increase of computational power, the attention to simplified models has decreased. On the other hand, through the years it became clear that simplified models have benefits over complex models because of their user friendliness, straight forward and fast calculation. These qualities are very suitable for integration in building simulation programmes. However, to obtain an accurate air temperature prediction in complex building design the models with distributed parameters, such as CFD, are more acceptable.

5. Conclusion

The simplified nodal models are analysed and validated with the experimental results in two measurement setups in order to evaluate the effect of different types and locations of heat loads, room height and office layout on the temperature gradient calculation in rooms with displacement ventilation. In all the treated cases displacement ventilation provides even temperature gradient throughout the simulated office room spaces.

Heat load distribution and accurate mixing height calculation are the most essential factors to predict the temperature stratification for the DV design conditions. In addition, the significant effect of room height and flow rates on the temperature gradient is revealed for the cases with high-level heat loads. Two-nodal model is not able to count these factors. Among the multi-nodal models Mateus and the presented nodal model demonstrate the closest temperature gradient prediction. The proposed nodal model is able to accurately calculate the all temperatures for all the typical room heights and indoor loads

References

- Arens, A. D. (2000). *Evaluation of Displacement Ventilation for Use in High-ceiling Facilities* (Mastes's Thesis). Retrieved from: <https://dspace.mit.edu/handle/1721.1/9305>
- Blaise, J. (2008). *Influence de la géométrie d'une source thermique sur le développement du panache* (Influence of the geometry of a thermal source on the development of the plume) (Doctoral dissertation). Retrieved from: <http://www.inrs.fr/inrs/recherche/etudes-publications-communications/doc/publication.html?reFINRS=C.7%2F1.037%2F4859%2FNS273>
- Bouzinaoui, A., Devienne, R., & Fontaine, J. R. (2007). An experimental study of the thermal plume developed above a finite cylindrical heat source to validate the point source model. *Experimental thermal and fluid science*, 31(7), 649–659.
- Chaengbamrung, A. (2005). *Turbulent plumes generated by a horizontal area source of buoyancy* (Doctoral dissertation). Retrieved from: <http://ro.uow.edu.au/theses/445/>
- Chen Q, Glicksman L, Yuan X, Hu S, Hu Y, & Yang X. (1999). *Performance evaluation and development of design guidelines for displacement ventilation*. (ASHRAE research project report RP-949). Atlanta: American Society of Heating, Ventilation and Air-Conditioning Engineers Inc. (US).
- Cooper, P., Hunt, G. R., & Linden, P. F. (2001, December). Transient flow in a ventilated enclosure containing a vertically distributed source of buoyancy. In *Proceedings of the 14th Australasian fluid Mechanics Conference* (pp. 449–452). Australia: Adelaide University.
- Davidson, G. A. (1986). Gaussian versus top-hat profile assumptions in integral plume models. *Atmospheric Environment* (1967), 20(3), 471–478.
- Devienne, R., & Fontaine, J. R. (2012). Experimental characterisation of a plume above rectangular thermal sources. Effect of aspect ratio. *Building and Environment*, 49, 17–24.
- Dokka, T. H. (2000). *Modelling of Indoor Air Quality in residential and commercial buildings*. (Doctoral dissertation). Retrieved from: <https://brage.bibsys.no/xmlui/handle/11250/265599>
- Espinosa, F. D., & Glicksman, L. R. (2017). Determining thermal stratification in rooms with high supply momentum. *Building and Environment*, 112, 99–114.
- Fontaine J. R., Devienne, & Rose S. (2006) Numerical Simulation and Experimental Validation of Plume Flow from a Heated Disk, Numerical Heat Transfer, Part A: Applications. *An International Journal of Computation and Methodology*, 50(7), 645–666
- Griffith, B. T. *Incorporating nodal and zonal room air models into building energy calculation procedures* (Mastes's Thesis). Retrieved from: <https://dspace.mit.edu/handle/1721.1/34970>

- Hunt, G. R., & Kaye, N. G. (2001). Virtual origin correction for lazy turbulent plumes. *Journal of Fluid Mechanics*, 435, 377–396.
- Hunt, G. R., & Van den Bremer, T. S. (2011). Classical plume theory: 1937 – 2010 and beyond. *IMA journal of applied mathematics*, 76(3), 424–448.
- Kaye, N. B., & Hunt, G. R. (2010). The effect of floor heat source area on the induced airflow in a room. *Building and Environment*, 45(4), 839–847
- Kosonen, R., Lastovets, N., Mustakallio, P., da Graça, G. C., Mateus, N. M., & Rosenqvist, M. (2016). The effect of typical buoyant flow elements and heat load combinations on room air temperature profile with displacement ventilation. *Building and Environment*, 108, 207–219.
- Kosonen R, Melikov A, Mundt E, Mustakallio P, & Neilsen PV (2017) *Displacement ventilation in non-industrial premises. REHVA Guidebook №23*. Forssa, Finland: Rehva.
- Li Y, Sandberg M, & Fuchs L. (1992). Vertical Temperature Profiles in Rooms Ventilated by Displacement: Full-Scale Measurement and Nodal Modelling. *Indoor Air* 2(4): 225–243.
- Mateus, N. M., & da Graça, G. C. (2015). A validated three-node model for displacement ventilation. *Building and Environment*, 84, 50–59.
- Menchaca Brandan, M. A. (2012) Study of airflow and thermal stratification in naturally ventilated rooms. (Doctoral dissertation). Retrieved from: <https://dspace.mit.edu/handle/1721.1/74907>
- Morton, B. R. (1959). The ascent of turbulent forced plumes in a calm atmosphere. *International journal of air pollution*, 1(3), 184–197.
- Mundt, E. (1995). Displacement ventilation systems – Convection flows and temperature gradients. *Building and Environment*, 30(1), 129–133.
- Nielsen, P. V. (2003, August). Temperature and air velocity distribution in rooms ventilated by Displacement Ventilation. In Kubota, H., Kobayashi, N., Tsuji, K., Enai, M. (Eds.), *Ventilation 2003, Proceedings of The 7th International Symposium on Ventilation for Contaminant Control* (pp 691–696) Sapporo: Hokkaido University.
- Novoselac A, Burley BJ, & Srebric J. (2006). Development of new and validation of existing convection correlations for rooms with displacement ventilation systems. *Energy and building*, 38, 163–173.
- Rees, S. J., & Haves, P. (2001). A nodal model for displacement ventilation and chilled ceiling systems in office spaces. *Building and Environment*, 36(6), 753–762.
- Skistad, H. (1994) *Displacement ventilation*. Taunton, UK: Research Studies Press Ltd.
- Zukowska, D., Melikov, A., & Popiolek, Z. (2007, June). Thermal plume above a simulated sitting person with different complexity of body geometry. In O. Seppänen, & J.

Säteri (Eds.), In *Proceedings of SCANVAC Conference Roomvent 2007* (pp. 191–198)
Helsinki: Finland Proceedings Abstract Book.